

# Sky Brightness Variation Measured at Auger Observatory

Andrew Newman

Advisors: Stefan Westerhoff, Michael Prouza

August 4, 2006

## Abstract

The fluorescence detectors at Auger Observatory have collected an unprecedented number of observations of the night sky brightness in the ultraviolet region of the spectrum. We have analyzed the temporal and spatial variation of this brightness and report trends in both. The overall U band sky brightness has decreased over the lifetime of the detector, likely due to a corresponding change in solar activity. Additionally, there are unexplained variations on the timescales of nights and months. The sky brightness also displays an elevation dependence which is well-modeled. Correlations between the fit parameters of this elevation dependence and atmospheric parameters were investigated; none were found. Finally, we present here the BGBrowser utility for viewing FD background frames and associated astronomical information.

## 1 Introduction

The Auger Observatory is designed to measure the energy spectrum and directional profile of the highest energy cosmic rays ( $E = 10^{18} - 10^{20}$  eV) in order to learn about their origins and potential acceleration mechanisms. The Observatory is a hybrid detector, ultimately consisting of 1600 Cherenkov water surface detectors and 24 UV fluorescence detectors (FDs) spread over 3000 km<sup>2</sup> in the *pampa amarilla* of western Argentina. Currently, 930 of the surface detectors and 18 of the fluorescence detectors are constructed and in operation. The flux of the highest energy cosmic rays is very low, approximately 1 particle km<sup>-2</sup> year<sup>-1</sup>, and measurements are dominated by poor statistics. Within its lifetime, the volume of data collected by the Observatory will surpass that of previous experiments by orders of magnitude.

When cosmic rays collide with the upper atmosphere, they produce a shower of secondary particles. These excite nitrogen atoms, causing them to emit UV photons, which are measured by the UV-sensitive telescopes in the Auger FDs. These data are used to reconstruct the shower development and determine the energy and atomic number of the incident particle. The 18 operational telescopes are divided among three sites at Coihueco, Los Leones, and Los Morados, which face inward along three sides of the surface detector area. Each site contains six bays, each containing a UV telescope which surveys approximately 30° of azimuth, allowing for a 180° field of view. Each telescope surveys elevations between 2° and 29° above the horizon. Imaging is performed by a 22 × 20 hexagonal grid of photomultiplier tubes (PMTs). The PMTs are periodically calibrated by illuminating them with a uniform UV light source and adjusting the response. For more information about the detector, see [1].

In addition to measurements triggered by cosmic ray showers, the FDs record background measurements of the night sky. An understanding of the sky background is interesting for several reasons. Tracking UV-bright stars has been used to align the pointing

Year	Data Coverage (s)	Observation Dark Time (s)	% Coverage
Coihueco			
2004	1968728	5218500	37.7%
2005	4310031	6075180	70.9%
2006	734774	2712600	27.1%
Los Leones			
2003	29590	1190040	2.5%
2004	2301477	5337360	43.1%
2005	2832793	6275400	45.1%
2006	658237	2510160	26.2%
Los Morados			
2005	3097293	4759140	65.1%
2006	443281	2354220	18.8%

Table 1: Data coverage as a fraction of dark time for each site. The Data Coverage column gives the total seconds of recorded data, in which each measurement represents 30 sec. The Observation Dark Time column gives the total seconds between astronomical sunset and sunrise for all nights during which data were taken.

of the telescopes [2]. The short-term variability must be checked to ensure that no false triggers originate from background fluctuations. It may be possible to extract atmospheric parameters from variations in the sky background, which would allow a check on other measurements important for shower reconstruction. Additionally, the physics of night sky brightness itself is not well understood, particularly in the U spectral band.

### 1.1 Sky brightness sources

The night sky brightness originates from sources both outside and within the atmosphere. Zodiacal light, light reflected from interstellar dust, and the integrated brightness of faint stars and galaxies are the main extraterrestrial components, in descending order of brightness. Within the atmosphere, most sky brightness is due to airglow emissions in an atmospheric layer at an altitude of about 100 km. This is caused by atoms and molecules in the upper atmosphere recombining after being ionized by solar radiation during the day. For more information on the components of night sky brightness, see [3].

## 2 Observations

The PMT electronics are AC coupled and thus do not allow for a direct measurement of the absolute photon flux. However, since the incoming photons obey Poisson statistics, the variance  $\chi^2$  in the signal is proportional to the photon flux. Each sky background measurement is an average of 65535 variances obtained at 100 ns intervals. Measurements are recorded every 30 sec [2]. It is possible to convert from the variance recorded to the actual photon flux (see [4]). However, for the purposes of this paper, it will be sufficient to retain the original variance units. The observational coverage for each site is shown in Table 1. These measurements do not account for the number of bays active at each site.

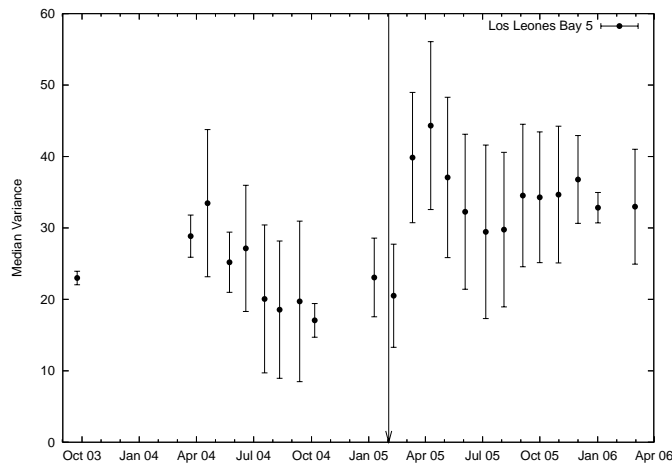


Figure 1: Period-median variances for Los Leones Bay 5 (see section 3.3 for the calculation procedure). The arrow shows the installation date of the corrector ring on 2 Feb 2005.

### 3 Time Variation

The night sky background flux is known to vary on many timescales, from over a single night to over the 11-year solar cycle. The mechanisms responsible for this often unpredictable variation are not well understood. In the FD background data, we have observed short-term (within a night) and long-term (over two years) variation, as well as possible intermediate-scale oscillations.

#### 3.1 Data selection and calculation

For this study, only data taken when the moon was at least  $0.5^\circ$  below the horizon (within a 3 min resolution) were used. Additionally, the data have been corrected for the installation of corrector rings. These rings are designed to eliminate coma aberration and increase aperture. They have gradually been installed at all FDs. From geometry, we expect the variance signal to be increased by a factor of 1.66 after the ring installation [5].<sup>1</sup> The variance data from each telescope have been adjusted to the corrector-ring equivalent by multiplying the variances obtained before the corrector ring was installed by 1.66. A sudden shift in the variance data around the time of installation is clearly seen in the uncorrected data, as shown in Figure 1. Finally, the average variance of each frame over all 440 pixels is calculated, excluding pixels with variances less than 0 (due to an electronics error) or greater than 100 (due either to an electronics error or to a very UV-bright star). Pixels containing UV-bright stars, which typically have variances less than 100, are not explicitly excluded from this average. However, their effect is not expected to be large. For instance, if all pixels were to have a variance of 30, except for a single pixel containing a star with variance 100, the mean would increase only to 30.2. Thus the effect of UV-bright stars on the frame mean is negligible compared the range of variation that is observed.

<sup>1</sup>Coihueco Bay 3 was the first bay to have a corrector ring installed. It is of lower quality, and the factor of 1.66 is not correct, which leads to low variance measurements at this bay.

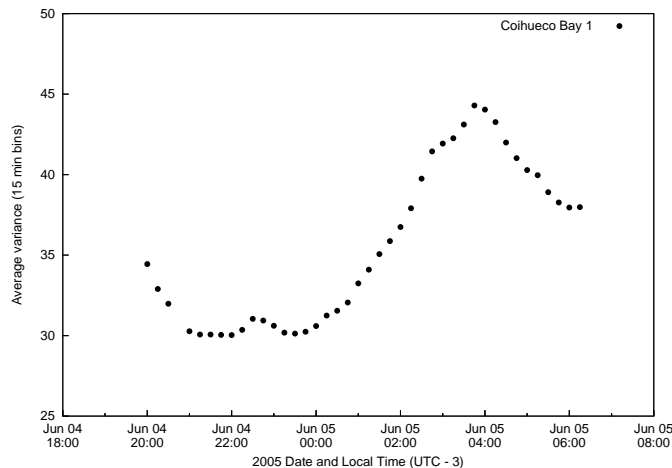


Figure 2: Variance change over one clear, moonless night as seen by Coihueco Bay 1. Similar curves were observed by all active bays at all sites during the same time period. Such nightly increases are not rare, but in fact are common in the data.

### 3.2 Nightly variation

On short time scales, the sky background measurements are quite stable, as should be expected based on the large number of variance readings that are averaged to produce each frame. Averaging over 10 frame (5 min) intervals, the typical frame-to-frame variation for a single pixel is 1-2%.

A variety of lightcurve of shapes are observed over different nights. Frequently there is a maximum, as seen in Figure 2. Initially we attributed this to variations in cloud cover, and in some cases the lightcurve shape may be correlated with cloud cover as seen in images obtained by sky cameras at Coihueco and Los Leones, though the correspondence is not completely compelling. However, significant increases in variance of 50% or more can be observed even on clear, cloudless nights. Figure 2 shows one such night as seen by Coihueco Bay 1. This night is among those confirmed clear in data provided by R. Clay et al. of the University of Adelaide (Australia), which were obtained by examining the sky camera images. A similar lightcurve is observed by all active bays at all sites during the same time period. Moreover, smooth increases of similar magnitude are observed over a number of clear, moonless nights (in fact, all that have thus far been examined). The cause of this is unknown. Comparisons with aerosol data collected by the Central Laser Facility did not reveal any clear correlation.

### 3.3 Long-term variation

To analyze the time variation of the data, observations from each bay at each site were grouped into observation periods, designed to correspond to the dark-time runs periods during which the FDs are in operation. In practice, observation periods are delineated in the data by gaps of one week or more. The frame means for each moonless background measurement are filtered to remove variances less than 10, since this typically indicates a closed bay door. The median variance over all measurements in the observation period is taken, and an error is estimated by taking half the spread of the middle 68% of the data. (The error is treated as symmetric, even though the median typically falls closer to the lower bound on the middle 68%.) Medians based on fewer than 400 measurements in the observation period, or on only one night of data, are discarded. The results of this procedure applied to Coihueco Bay 4 and Los Leones Bay 4 are shown in Figure 3.

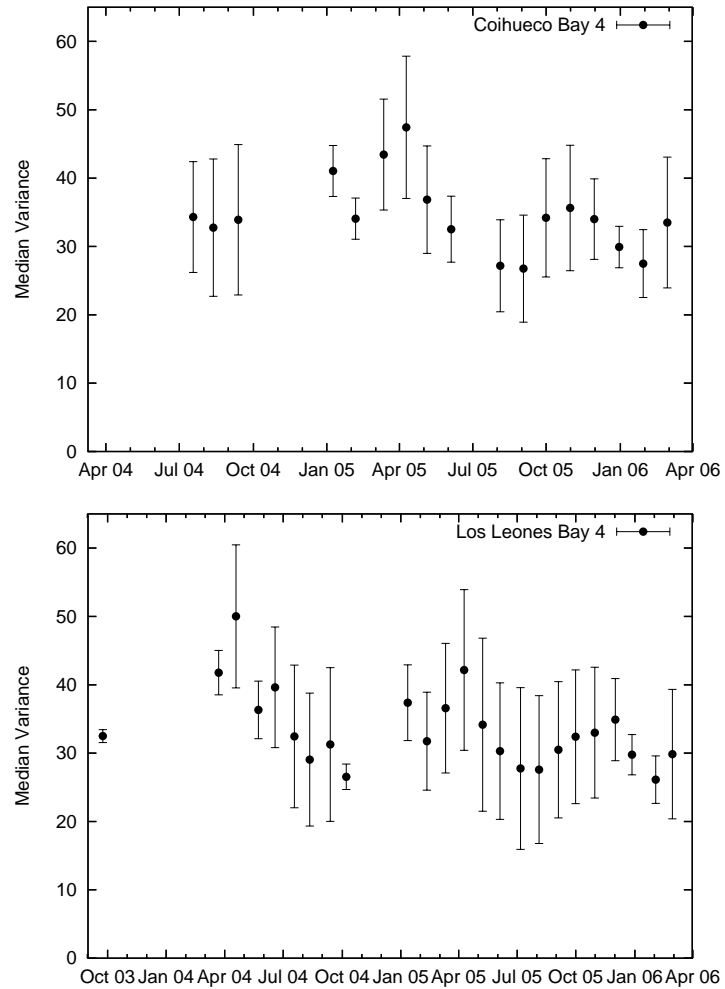


Figure 3: Period-median variances for Coihueco Bay 4 (left) and Los Leones Bay 4 (right). Error bars show the spread of the middle 68% of the data.

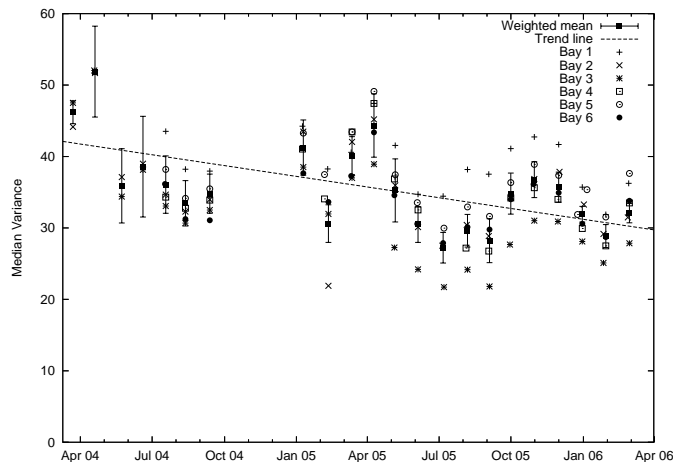


Figure 4: Period-median variances for all bays at Coihueco and their weighted mean. Error bars on the mean are obtained by treating the 68%-spread error bars on the individual bays as standard  $\sigma$ . The dashed line shows a trend line with slope  $a = -6.02 \pm .79 \text{ year}^{-1}$ .

Variance measurements from different bays at the same site have different intrinsic levels. This is due both to different azimuth pointing directions (for instance, some bays face near to light pollution originating from Malargüe, while others face directly away) and possible instrumental differences. However, the relative changes are generally the same across all bays. Thus we can take a mean over all bays to reflect the sky background at the site as a whole and obtain better statistics. To do so, the period medians for each bay are binned into observation periods as described above, and the weighted mean is calculated for each period. The error estimated from the 68%-spread previously described is used for weighting. Figure 4 shows the period-medians for each bay at Coihueco and their weighted means. A general decreasing trend is apparent. To illustrate this pattern, a linear trend line is also plotted.

Although the data plotted in Figures 3 and 4 is moonless, it is not necessarily cloudless. Extensive cloud cover in moonless nights significantly reduces the variance. Variances as low as 15 have been observed. Currently there is no bay-by-bay cloud cover data available, which makes it impossible to properly filter the background variances for clear conditions. General cloud cover estimates, nevertheless, have been obtained by R. Clay et al., who provide a list of confirmed clear nights. For the Coihueco site, there are 30 such nights. These clear nights were subjected to the same analysis as the full data set, with the exception that no cut is made based on the number of measurements or number of nights within an observation period. The result is shown in Figure 5. The solid line shows the weighted mean over all bays, and the dashed line shows the analogous mean obtained from data over all nights, as shown in Figure 4. Although the absolute variances sometimes differ greatly, which should be expected given the very small number of clear nights, the general trend is the same. This suggests that the long-term sky brightness variations are not attributable to weather alone.

Figure 6 shows the weighted means for each observation period over all bays for Coihueco, Los Leones, and Los Morados. Despite the wide variation seen over bays at an individual site, the overall site means generally agree well, particularly during the last year of data. Figure 6 also shows the weighted mean over all sites during each observation period and a linear trend line. The slope deviates from zero by  $11.6\sigma$ .<sup>2</sup> The good agree-

<sup>2</sup>It is possible that combining the 68%-spread errors from individual bays in the usual way gives an unrealistically low error to the mean data points and hence the trend line slope.

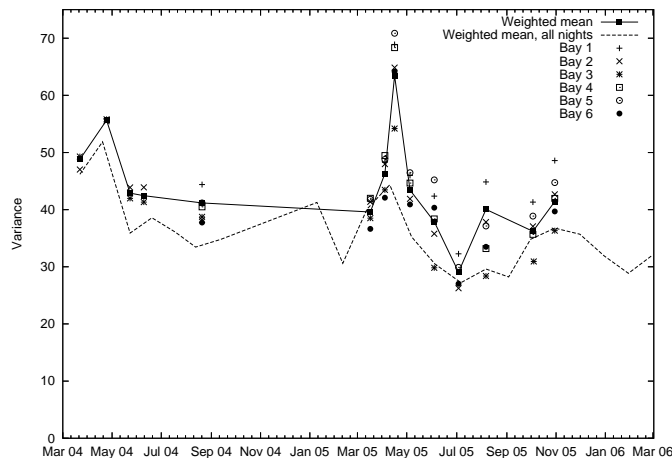


Figure 5: Period-median variances for all bays at Coihueco using 30 clear nights only. The dashed line shows their weighted mean, and the dashed line shows the analogous weighted mean obtained using all nights, as shown in Figure 4. Although the absolute values are not identical, which should be expected given the small number statistics here, the relative changes are similar whether all nights or only clear nights are included.

ment among all sites suggests the decreasing trend is real and not due to instrumental effects.

Again, a general decrease in variance is apparent in all plots. It is possible that much of the long-term decrease is due to variations in the solar cycle. Solar activity is known to significantly affect airglow, the dominant component of night sky brightness. Numerous studies have demonstrated some correlation between sky brightness and solar activity. Rayleigh first reported a correlation between the intensity of the [OI] airglow line and the number of sunspots in 1928 [6]. Walker later reported a correlation between the broadband  $V$  and  $B$  fluxes and night sky brightness, as measured by the 10.7 cm solar radio flux [7]. He also speculated that the night sky brightness could be predicted based on solar activity during the previous day. Subsequent studies have supported a long-term correlation of sky brightness and solar activity while rejecting a short-term (i.e., night-to-night) dependence [8, 9, 10]. Interestingly, two studies have reported positive correlations in all bands except U, in which an anti-correlation is suggested [8, 10]. However, these studies have very little data in this spectral region, so little can be concluded. Our data do not support a negative U band correlation.

The period during which the FDs have been collecting data corresponds to a decreasing period of the solar cycle. Data obtained from the National Geophysical Data Center (NGDC)<sup>3</sup> show that the 10.7 cm solar flux decreased from 151.3 in October 2003 to 89.0 in April 2006. Figure 7 shows the all-site mean variance and solar fluxes at both 10.7 cm and in the FUV. The FUV data were measured by the Solar Extreme Ultraviolet Monitor.<sup>4</sup> Clearly there is no tight correlation, but there does seem to be agreement in the general decrease of night sky brightness along with solar activity. At present this is our best hypothesis. We will be able to judge better once the solar minimum has been passed in two years.

There seems to be additional oscillatory variation in Figure 6 in addition to the long-term decreasing trend. It seems to be approximately seasonal with decreasing amplitude.

<sup>3</sup>[ftp://ftp.ngdc.noaa.gov/STP/SOLAR\\_DATA/SOLAR\\_RADIO/FLUX/MONTHLY.OBS](ftp://ftp.ngdc.noaa.gov/STP/SOLAR_DATA/SOLAR_RADIO/FLUX/MONTHLY.OBS)

<sup>4</sup>[http://www.usc.edu/dept/space\\_science/semdatafolder/long/daily\\_avg/](http://www.usc.edu/dept/space_science/semdatafolder/long/daily_avg/)

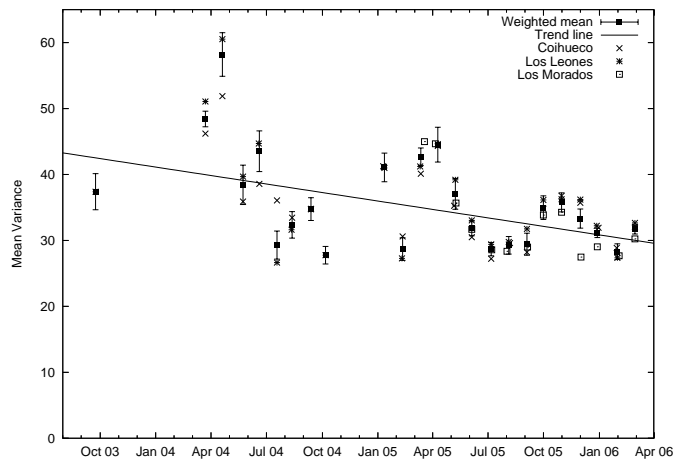


Figure 6: Weighted mean variances for all sites, obtained as in Figure 4, and their weighted means. The dashed line is a trend line with slope  $5.14 \pm 0.44 \text{ year}^{-1}$ .

This would be quite interesting, since the only previous study of which we are aware that has investigated such intermediate-range correlations reported none [10]. From weather, one would expect more clouds in the winter months and hence lower variances. However, the opposite trend appears in the data. After more background data is obtained in the coming years, it will be easier to judge whether any seasonal effect actually exists.

## 4 Elevation dependence

The night sky brightness originates both from astronomical sources, such as zodiacal light and the integrated light from faint stars and galaxies, and from airglow emission in the van Rhijn layer of the atmosphere. The latter contribution is dominant. Although we expect airglow to be roughly independent of azimuth, it does vary with elevation, since at different elevations the path length along the line of sight through the emitting layer varies. In particular, angles near the horizon have the highest airmass and hence stronger airglow. Garstang has constructed a simple model for this elevation dependence [11].

Suppose airglow is the source of a fraction  $f$  of night sky brightness. Letting  $b_i(Z)$  be the sky brightness at a zenith angle  $Z$ , as seen just below the emitting layer of the atmosphere, we can write

$$b_i(Z) = b_0[(1 - f) + fX]. \quad (1)$$

Here  $b_0$  is the brightness at the zenith, and  $X(Z)$  measures the path length along the line of sight, known as the airmass, which is given by

$$X = (1 - 0.96 \sin^2 Z)^{-1/2}. \quad (2)$$

The  $(1 - f)$  term in Equation (1) represents the constant contribution of sources outside the atmosphere, which does not vary with elevation. The  $fX$  term represents the airglow contribution, which increases with airmass and hence with  $Z$ .

To determine the observed sky brightness on the ground we must account for extinction that occurs between the airglow layer of the atmosphere and the ground. Letting  $\kappa$  be the UV-band extinction coefficient (in mag airmass $^{-1}$ ), extinction should decrease the magnitude by  $\Delta m = \kappa X$ . The extinction relative to the zenith is then  $\delta m = \kappa(X - 1)$ , which corresponds to a factor in brightness of  $10^{-0.4\kappa(X-1)}$ . Letting  $b_0$  now represent the

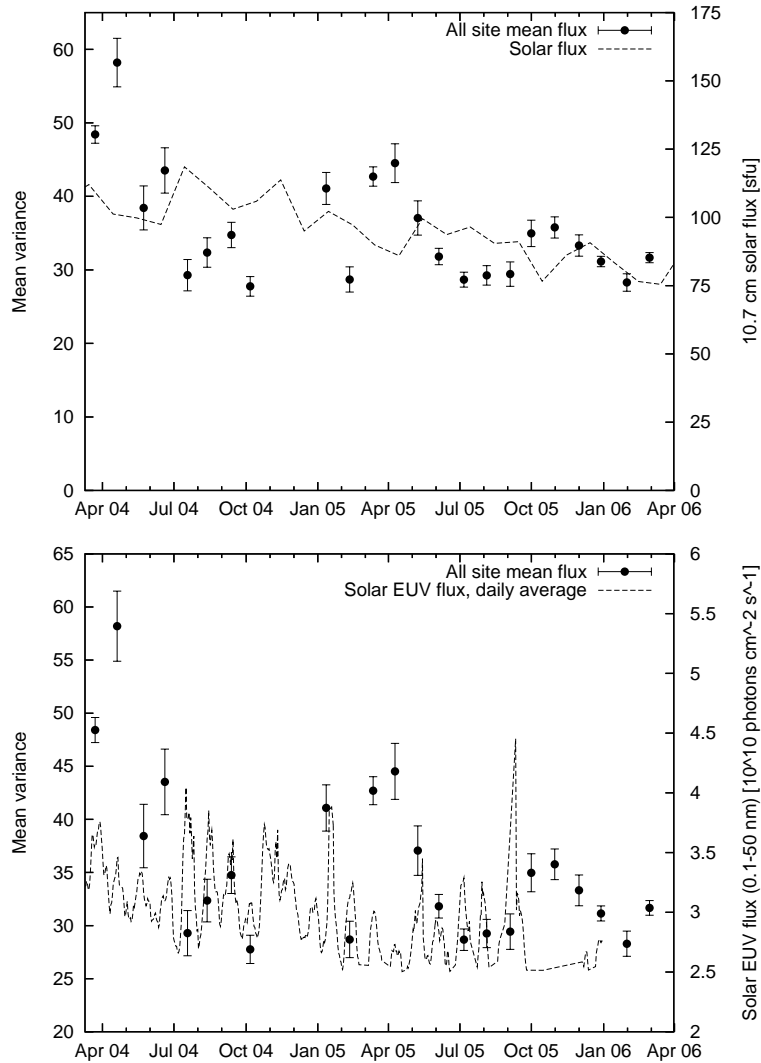


Figure 7: All site mean variances, as shown in Figure 6, plotted against two solar flux measurements. On the left, the 10.7 cm solar radio flux recorded by the NGDC. On the right, the far ultraviolet flux (0.1 - 50 nm) recorded by the Solar Extreme Ultraviolet Monitor.

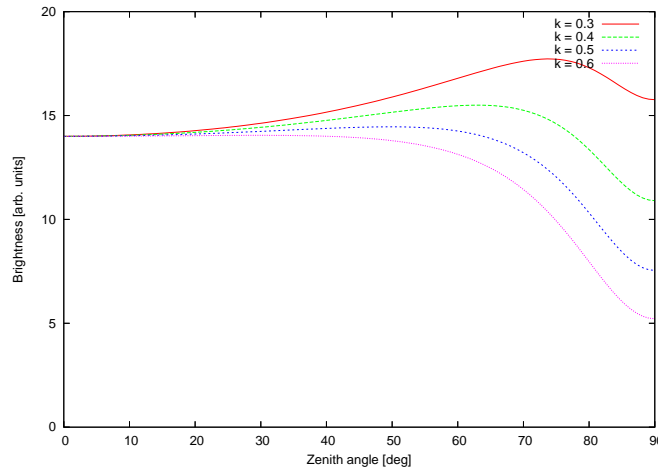


Figure 8: Theoretical sky brightness dependence on elevation for several values of the extinction coefficient  $\kappa$ . The parameters  $b_0 = 14$  and  $f = 0.6$  are fixed.

observed brightness at the zenith *after* extinction, it follows that the sky brightness as a function of zenith angle  $Z$  is given by

$$b(Z) = b_0[(1 - f) + fX]10^{-0.4\kappa(X-1)}. \quad (3)$$

We have adopted  $f = 0.6$  (i.e., 60% of night sky brightness is due to airglow), following for instance [11], [3], and [10]. A plot of  $b(Z)$  using  $b_0 = 14$ ,  $f = 0.6$ , and several values of  $\kappa$  is shown in Figure 8.

We can try to fit the observed dependence of variation on elevation with this functional form. Each row of PMTs is at approximately constant elevation (within  $< 0.1^\circ$ ). Thus, for each frame of data, we can take the average variance for each row, again excluding variances  $< 0$  or  $> 100$ . By cutting nights which have a lunar illumination greater than 10% and averaging over all all bays at all three sites, we get the elevation profile shown in Figure 9. (Each data point is a row whose average elevation is the horizontal coordinate.) The fit shown has  $b_0$ ,  $k$ , and  $f$  as free parameters. Note that the best-fit  $\kappa$  and  $f$  have values in the expected range. The row with lowest elevation (highest zenith angle) shows the greatest deviation from the fit. This can be expected, since the derivation of Equation (3) does not account for effects such as multiple scattering which become significant at high airmasses.

We can use this typical elevation variation to “flat-field” the camera in the following way. For each row, determine the fractional contribution  $f_r$  to the total variance. If all rows contributed equally, this value would be  $1/22$  for every row. We define a factor  $c_r = \frac{1/22}{f_r}$  for each row and multiply all variances in the row by  $c_r$ . This effectively increases the variances on the lower rows, which are suppressed by high airmasses, and lowers the variances on the higher rows, while preserving the average variance over the whole frame. Figure 10 shows a raw data frame on the left and the same frame flattened by this procedure on the right. (The flattening was performed using row averages over the entire data file in which this frame is located, i.e. the majority of one night of data. Since atmospheric conditions vary, this procedure usually results in better flattening than universally applying the overall means shown in Figure 9.)

Since  $\kappa$  is a measure of atmospheric extinction, we can hope to use it as a measure of current atmospheric conditions. Atmospheric data has also been obtained by the Central Laser Facility (CLF), which has measured  $\alpha$ , an indicator of the aerosol content in the atmosphere, several times a night for a many nights. We investigated possible correlations

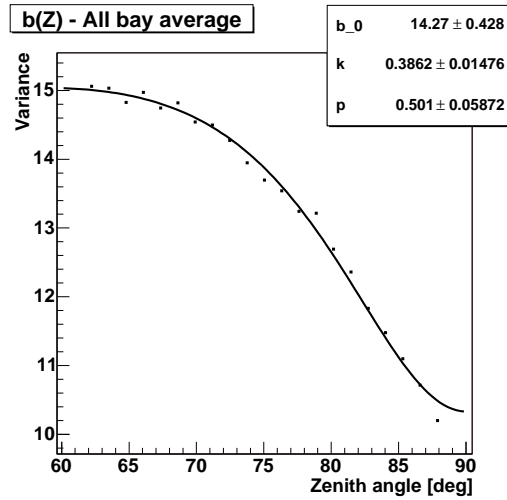


Figure 9: Row-averaged variances averaged over all bays at all FD sites over the entire data period. The fit shown is Equation 3 with  $b_0$ ,  $k$ , and  $f$  as free parameters. ( $p$  in the figure is the same as  $f$ .)

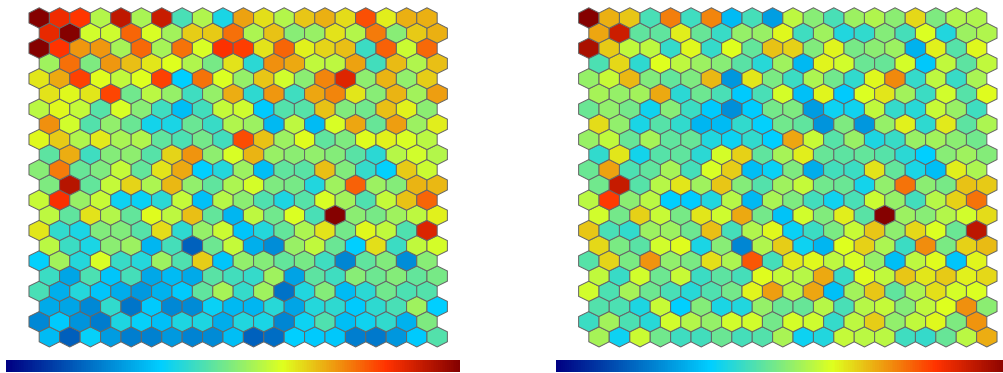


Figure 10: A single variance frame taken at 23:28:58 04 JUN 2005 (local time, UTC - 3) by Coihueco Bay 3. The left image shows the raw data frame, and the right image shows the same frame flattened using row elevation data averaged over the entire data file. This removes the gradient from lower (bluer) fluxes at the bottom of the frame to higher (redder) fluxes at the top, which is due to differences in airmass along different lines of sight for each row. The very bright pixel in the ninth row from the bottom is due to a UV-bright (first magnitude) star.

between  $\alpha$  and the  $\kappa$  obtained for a fit over ten frames surrounding the time of the laser measurement. No correlation was found.

## 5 Variation in the variation of the variance

Another potential indicator of atmospheric and weather conditions which we investigated is the RMS of the variance across each frame. Very clear or completely cloudy nights should have a low RMS, while partly cloudy nights should have a high RMS. No correlation was found between the RMS and  $\alpha$ . The RMS of each frame as a fraction of the mean frame variance was also used as a statistic. Again, no correlation was found with  $\alpha$ , nor was any correlation found between the time derivatives of the RMS or fractional RMS and  $\alpha$ . The mean fractional RMS is 20% with an RMS of 12%.

## 6 BGBrowser

To help visualize the background data from the FDs, M. Santander, M. Prouza, S. Ben-Zvi, and the author have developed the BGBrowser utility, which plots background data frames, both raw and flat-fielded, as seen in Figure 10. The color palette and scale are adjustable by the user. The program is capable of tracking stars (using a catalog) and planets across the camera, as well as displaying moon ephemeris for each frame. It displays the elevation, azimuth, and variance of each pixel, and it can produce plots of the variance in a single pixel across an entire data file. Single frames may be saved in a variety of graphics formats, and animated GIFs may be created. This tool may be used to monitor status of the FDs. Electronic errors, such as bad columns and dead pixels, are clearly visible.

## 7 Conclusions

We have detected time variation in the sky background on several scales, from nightly variations to a decrease over the two years of observation. Large variation (50%) over individual clear nights remains unexplained. The long-term variation seems to be related to decreasing solar activity in the current phase of the solar cycle, although the correlation is not simple. There seems to be an intermediate-term, possibly seasonal, effect in addition to the long-term decrease, whose origin is also unknown.

We have also observed a systematic elevation dependence which is well-described by a simple model. By fitting the data to this model we obtain information on atmospheric parameters. It seems difficult to correlate these in a systematic way to data obtained by the Central Laser Facility. Additionally, the RMS spread in the frame variance does not correlate well with CLF data.

The BGBrowser program presented here is a useful tool for displaying background frames. It allows rapid review of frames over a night and may also be used to easily detect electronics errors.

## 8 Acknowledgments

A. Newman thanks S. Westerhoff, M. Prouza, S. BenZvi, and B. Connolly for the guidance and mentorship, as well as the National Science Foundation for their support via the Research Experience for Undergraduate (REU) program.

## References

- [1] Auger Collaboration: **Pierre Auger Project Technical Design Report**, <http://tdpc01.fnal.gov/auger/org/tdr/index.html>.
- [2] C. De Donato, F. Sanchez, M. Santander, D. Camin, B. Garcia & V. Grassi: **Using star tracks to determine the absolute pointing of the Fluorescence Detector telescopes**, GAP note 2005–008.
- [3] C.R. Benn & S.L. Ellison: **La Palma night-sky brightness**, [http://www.ing.iac.es/Astronomy/observing/manuals/ps/tech\\_notes/tn115.ps.gz](http://www.ing.iac.es/Astronomy/observing/manuals/ps/tech_notes/tn115.ps.gz)
- [4] R. Caruso, et al.: **Measurement of the sky photon background flux at the Auger Observatory**, Proceedings of the 29th International Cosmic Ray Conference, Pune, pp. 101–106, 2005.
- [5] R. Caruso & S. Petrera: **Measurement of the sky photon background flux at Los Leones**, GAP Note 2004–072.
- [6] Lord Rayleigh IV (R.J. Strutt), Proc. Roy. Soc. London A, vol. 119, p. 11, 1928.
- [7] M.F. Walker: **The effect of solar activity on the V and B band sky brightness**, Pub. Astron. Soc. Pacific, vol. 100, pp. 496–505, 1988.
- [8] C. Leinert, et al.: **Measurements of sky brightness at the Calar Alto Observatory**, Astron. Astrophys. Suppl., vol. 112, pp. 99–121, 1995.
- [9] K. Matilla, et al.: **Sky brightness at the ESO La Silla Observatory 1978 to 1988**, Astron. Astrophys. Suppl., vol. 119, pp. 153–170, 1996.
- [10] F. Patat: **UBVRI night sky brightness during sunspot maximum at ESO-Paranal**, Astron. Astrophys., vol. 400, pp. 1183–1198, 2003.
- [11] R.H. Garstang: **Night-sky brightness at observatories and sites**, Pub. Astron. Soc. Pacific, vol. 101, pp. 306–329, 1989.